GFZ
Helmholtz-Zentrum
POTSDAM

Originally published as:

Roth, D. L., Finnegan, N. J., Brodsky, E. E., Rickenmann, D., Turowski, J., Badoux, A., Gimbert, F. (2017): Bed load transport and boundary roughness changes as competing causes of hysteresis in the relationship between river discharge and seismic amplitude recorded near a steep mountain stream. - *Journal of Geophysical Research*, *122*, 5, pp. 1182—1200.

DOI: http://doi.org/10.1002/2016JF004062

AGU PUBLICATIONS

JGR

Journal of Geophysical Research: Earth Surface

RESEARCH ARTICLE
10.1002/2016JF004062

Key Points:
- Hysteresis in seismic signals near rivers may not always indicate hysteresis in bed load sediment transport rates, as previously assumed
- The seismic signal generated by water turbulence, rather than sediment transport, can dominate seismic observations near rivers
- Shifting of grains on the river bed may change the seismic response to fluid flow between rising and falling water levels (hysteresis)

Correspondence to:
D. L. Roth,
danicalir@gmail.com

Citation:
Roth, D. L., N. J. Finnegan, E. E. Brodsky, D. Rickenmann, J. M. Turowski, A. Badoux, and F. Gimbert (2017), Bed load transport and boundary roughness changes as competing causes of hysteresis in the relationship between river discharge and seismic amplitude recorded near a steep mountain stream, *J. Geophys. Res. Earth Surf.*, *122*, 1182–1200, doi:10.1002/2016JF004062.

Received 30 AUG 2016
Accepted 27 APR 2017
Accepted article online 1 MAY 2017
Published online 26 MAY 2017

©2017. American Geophysical Union. All Rights Reserved.

Bed load transport and boundary roughness changes as competing causes of hysteresis in the relationship between river discharge and seismic amplitude recorded near a steep mountain stream

Danica L. Roth[1], Noah J. Finnegan[1], Emily E. Brodsky[1], Dieter Rickenmann[2], Jens M. Turowski[3], Alexandre Badoux[2], and Florent Gimbert[4]

[1]Department of Earth and Planetary Sciences, University of California, Santa Cruz, California, USA, [2]WSL Swiss Federal Institute for Forest, Snow and Landscape Research, Birmensdorf, Switzerland, [3]GFZ German Research Centre for Geosciences, Potsdam, Germany, [4]University of Grenoble Alpes, CNRS, IRD, IGE, Grenoble, France

Abstract Hysteresis in the relationship between bed load transport and river stage is a well-documented phenomenon with multiple known causes. Consequently, numerous studies have interpreted hysteresis in the relationship between seismic ground motion near rivers and some measure of flow strength (i.e., discharge or stage) as the signature of bed load transport. Here we test this hypothesis in the Erlenbach stream (Swiss Prealps) using a metric to quantitatively compare hysteresis in seismic data with hysteresis recorded by geophones attached beneath steel plates within the streambed, a well-calibrated proxy for direct sediment transport measurements. We find that while both the geophones and seismometers demonstrate hysteresis, the magnitude and direction of hysteresis are not significantly correlated between these data, indicating that the seismic signal at this site is primarily reflecting hysteresis in processes other than sediment transport. Seismic hysteresis also does not correlate significantly with the magnitude of sediment transport recorded by the geophones, contrary to previous studies' assumptions. We suggest that hydrologic sources and changes in water turbulence, for instance due to evolving boundary conditions at the bed, rather than changes in sediment transport rates, may sometimes contribute to or even dominate the hysteresis observed in seismic amplitudes near steep mountain rivers.

Plain Language Summary An increasing number of studies have recently observed changes in the amount of seismic shaking (hysteresis) recorded near a river at a given discharge during floods. Most studies have assumed that this hysteresis was caused by changes in the amount of sediment being transported in the river and have therefore used the hysteresis to assess sediment transport rates and patterns. We examine concurrent seismic and sediment transport data from a steep mountain stream in the Swiss Prealps and find that changes in seismic shaking are unrelated and even opposed (increasing versus decreasing) to changes in sediment transport rates for four out of five transport events. Water turbulence, rather than sediment transport, appears to be the strongest source of seismic shaking, and changes in seismic shaking are most likely caused by changes in turbulence or how turbulence transmits energy through the river bed. These effects may be due to rearrangement of sediment around large boulders on the bed or slight shifting of the boulders themselves. Our results have significant implications for the growing field of fluvial seismology and the evaluation of seismic data near rivers, as previous interpretations of seismic hysteresis as evidence for sediment transport may not always be accurate.

1. Introduction

The transport of coarse bed load sediment in rivers is a key process governing fluvial morphodynamics and geomorphology. Understanding when sediment moves and assessing sediment transport rates are crucial to predicting channel evolution and addressing a wide range of problems in fields including ecology, land use management, and civil engineering. However, sediment transport is a highly nonlinear and stochastic process, making it notoriously challenging to assess. A prime example of this nonlinearity is the well-documented phenomenon of hysteresis in the relationship between the rate of coarse sediment transport and some measure of river flow strength, such as water discharge or stage. Such hysteresis has been observed over timescales ranging from hours to years and in both clockwise (greater transport on rising limb of the hydrograph) [e.g., *Allen*, 1974; *Nanson*, 1974; *Walling*, 1977; *Dunne and Leopold*, 1978; *Moog and Whiting*, 1998] and

counterclockwise (greater transport on falling limb) [e.g., *Klingeman and Emmett*, 1982; *Emmett et al.*, 1983; *Milhous and Klingeman*, 1992] directions, although clockwise observations are much more common. Hysteresis in sediment transport is generally argued to reflect exhaustion or increases in sediment supply [e.g., *Nanson*, 1974; *Dunne and Leopold*, 1978; *Reid et al.*, 1985; *Moog and Whiting*, 1998; *Whiting et al.*, 1999; *Topping et al.*, 2000; *Wulf et al.*, 2012; *Mao et al.*, 2014] or changes in transport efficiency due to structural evolution of the bed, such as packing [e.g., *Charru et al.*, 2004; *Mao*, 2012], bed form evolution [*Martin and Jerolmack*, 2013], or changing the grain size of the bed surface [e.g., *Dietrich et al.*, 1989; *Kuhnle*, 1992; *Whiting et al.*, 1999; *Wohl and Cenderelli*, 2000; *Kleinhans et al.*, 2007; *Humphries et al.*, 2012].

The challenges inherent in monitoring transport in situ limit understanding and study of hysteresis in coarse sediment transport rates. Recently, however, seismology has emerged as a promising new means of monitoring bed load transport via the elastic waves generated by impacts between mobile sediment and the river bed [e.g., *Burtin et al.*, 2011; *Tsai et al.*, 2012; *Burtin et al.*, 2016; *Schmandt et al.*, 2017]. Numerous studies have reported hysteresis in the relationship between seismic power recorded near rivers and discharge or stage, which is argued to reflect underlying changes in sediment transport rates [e.g., *Govi et al.*, 1993; *Burtin et al.*, 2008, 2010; *Hsu et al.*, 2011; *Schmandt et al.*, 2013; *Roth et al.*, 2014; *Chao et al.*, 2015; *Barrière et al.*, 2015]. Seismic hysteresis near rivers has been observed over timescales ranging from single flood events [e.g., *Hsu et al.*, 2011] to seasons [e.g., *Burtin et al.*, 2008]. *Burtin et al.* [2008] found clockwise seasonal hysteresis in seismic power in the 1–20 Hz frequency band near the Trisuli River in the Himalayas, which was attributed to the ground vibrations generated by coarse sediment transport. In both aggradational and erosional flood events on the Cho-Shui River in central Taiwan, *Hsu et al.* [2011] found a consistent clockwise hysteresis between seismic amplitude (1–9 Hz frequency) and river stage, which they proposed to represent a decrease in transport efficiency due to temporal evolution of the channel bed. Similar clockwise hysteresis has been reported by *Chao et al.* [2015] on the Chishan River in Taiwan (5–15 Hz frequency). On the Chijiawan River in northern Taiwan, *Roth et al.* [2014] demonstrated that the magnitude of seismic hysteresis in the 1–45 Hz frequency band was strongly correlated with sediment transport patterns and tracked the downstream migration of a sediment pulse released following a dam removal.

These studies suggest that in the absence of direct observations of the channel bed, the continuous, high temporal resolution record provided by seismic data can offer new insight into bed load transport processes. However, the degree to which seismic hysteresis represents changes in sediment transport rates, and how this may vary with hydrologic and fluvial parameters, has yet to be established. In particular, many studies [e.g., *Burtin et al.*, 2008; *Hsu et al.*, 2011; *Schmandt et al.*, 2013; *Roth et al.*, 2014; *Díaz et al.*, 2014] have relied on the assumption that sediment transport is the sole or dominant process causing hysteresis in the seismic signal and that the seismic signal generated by fluid flow over the bed does not experience significant, if any, additional hysteresis. While several studies have noted that fluid processes may influence the magnitude of seismic hysteresis generated by bed load [e.g., *Gimbert et al.*, 2014; *Roth et al.*, 2014; *Barrière et al.*, 2015] or that turbulent fluid flow alone may generate seismic hysteresis [*Gimbert et al.*, 2016], whether or not turbulent fluid flow can directly generate seismic hysteresis in an open channel flow has not yet been explored. *Gimbert et al.* [2014] developed a quantitative model for the seismic signal generated by turbulent fluid flow in rivers and demonstrated that the magnitude of observed seismic hysteresis depends strongly on the relative strengths of the sediment transport (the assumed source of hysteresis) and turbulent flow signals. In typical Himalayan river settings, for example, they propose that the seismic source generated by turbulent fluid flow can be large enough that bed load hysteresis may not be fully recovered in the seismic signal [*Gimbert et al.*, 2014]. On the Colorado River, *Schmandt et al.* [2013] distinguished active spectral bands thought to be generated by either sediment transport (15–45 Hz) or fluid processes (0.5–15 Hz) based in part on the presence of clockwise hysteresis in the 15–45 Hz band; a weaker counterclockwise hysteresis was observed in the 2–15 Hz band and was suggested to represent a change in the surface water wave pattern due to the movement of bed load. *Barrière et al.* [2015] concluded that the clockwise hysteresis they observed in 10–80 Hz band-averaged seismic power was mainly the result of hysteresis in bed load transport, although they noted that hysteresis in fluid shear velocity could also have contributed to this effect.

Here we use dedicated observations in a relatively small mountain stream to demonstrate that (1) water turbulence rather than sediment transport can dominate the seismic signal and (2) seismic power and bed load transport rates can exhibit hysteresis in opposing directions, which we suggest may reflect hysteresis in the water turbulence signal due to changing boundary conditions at the bed. We use a modified

version of the hysteresis metric Ψ developed by *Roth et al.* [2014] to examine the magnitude of hysteresis measured by a seismometer installed on the bank of the Erlenbach, a small, steep alluvial stream in the Swiss Prealps [*Roth et al.*, 2016]. This hysteresis shows no significant correlation with the hysteresis observed in proxy sediment transport rates recorded by geophones embedded in the channel bed. We show that both the magnitude and direction (clockwise or counterclockwise) of hysteresis varies inconsistently between the seismic and geophone data, indicating that the hysteresis recorded in seismic records may sometimes represent changes in seismic sources other than sediment transport, contrary to previous studies' assumptions. We discuss possible causes of hysteresis in the seismic signal generated by both sediment transport and water turbulence and provide a quantitative illustration of the seismic effects of changing mean grain-scale bed roughness and/or changing flow velocity due to changes in large-scale roughness.

2. Study Site and Data

The Erlenbach was selected as our field site due to the presence of extensive monitoring infrastructure, which enables independent constraints on water discharge and sediment transport. The Erlenbach is equipped with an in-bed Swiss plate geophone system installed at the downstream end of an ~40 m long engineered concrete-bed reach (Figure 1), which has provided continuous, reliable sediment transport measurements since 2002 [*Turowski et al.*, 2009, 2011; *Rickenmann and Fritschi*, 2010; *Rickenmann et al.*, 2012, 2014]. This system consists of six geophones attached beneath elastically isolated steel plates (each 0.36 m × 0.5 m × 0.015 m) embedded flush with the channel bed. The geophone system records the vibrations generated by impacts of grains larger than ~10 mm [*Rickenmann et al.*, 2012]. The number of impulses (peaks exceeding a threshold value) per minute is recorded for each geophone. Sediment generally becomes mobile at discharges greater than ~0.15 m^3/s [*Turowski et al.*, 2011]. Immediately downstream of the geophones lies an engineered waterfall into a retention basin (~30 m × 15 m); this basin has been regularly surveyed to constrain long-term sediment export since 1982. Short-term sediment transport rates have been monitored since 2009 with measurements from automated basket samplers that move into the waterfall during transport events [*Rickenmann et al.*, 2012]. Previous studies have used these measurements to empirically calibrate a linear relationship between geophone impulses and sediment volume or mass [*Rickenmann et al.*, 2012; *Beer et al.*, 2015]. This correlation is excellent ($r^2 \geq 0.91$) [*Rickenmann et al.*, 2012; *Beer et al.*, 2015] for 1 min data and improves when measurements are averaged over several minutes [e.g., *Rickenmann and McArdell*, 2008].

Stage data are continuously collected at 1 min intervals by a gauging station ~35 m upstream of the geophones and ~5 m downstream from the start of the engineered concrete bed (Figure 1). Discharge is then calculated from the stage data using a calibrated stage-discharge relationship [e.g., *Beer et al.*, 2015]. Immediately downstream of the gauging station, the flow drops over an engineered overfall structure (~1 m high) into a shallow stilling basin (~4 m × 4 m × 0.3 m depth), then enters a fairly smooth ~30 m engineered concrete reach with embedded riprap before reaching the geophones.

Our study site is an alluvial step-pool reach immediately upstream of the engineered reach containing the geophones and gauging station. The channel here has a mean elevation of 1114 m above sea level, a drainage area of 0.7 km^2, a mean bed slope of 0.1 [*Turowski et al.*, 2011], and an average width of ~5 m. This reach has partially engineered banks reinforced with meter-sized boulders from the channel to form a roughly rectangular cross section. Grains range in size from clay to meter-sized boulders, with a median grain size, D_{50}, of ~80 mm [*Turowski et al.*, 2011]. The study reach is located on a large landslide complex, and colluvial sediment is supplied to the channel by very active hillslopes [*Schuerch et al.*, 2006; *Turowski et al.*, 2011; *Golly et al.*, 2017] composed of Wägital Flysch bedrock consisting of interbedded mudstone and sandstone, with occasional limestone clasts [*Winkler et al.*, 1985].

From 6 July to 1 September 2013, we installed a Sercel L-28 3-channel high-frequency seismometer on the bank of the Erlenbach. Installation was at approximately 1 cm depth (instrument top to surface) in a primarily sand and mud soil substrate, ~4 m from the channel thalweg, and ~60 m and ~25 m upstream of the geophones and gauging station, respectively [*Roth et al.*, 2016]. The instrument was placed ~20 m equidistant from an upstream tributary junction and the start of the engineered concrete-bed reach downstream, at roughly the midpoint of an ~8 m long straight reach between large boulders. We examine the horizontal stream-parallel (east-west) component of ground motion in the 35–55 Hz band, which *Roth et al.* [2016] found to contain the strongest signal of bed load transport. Our data were sampled at 1 kHz, from which

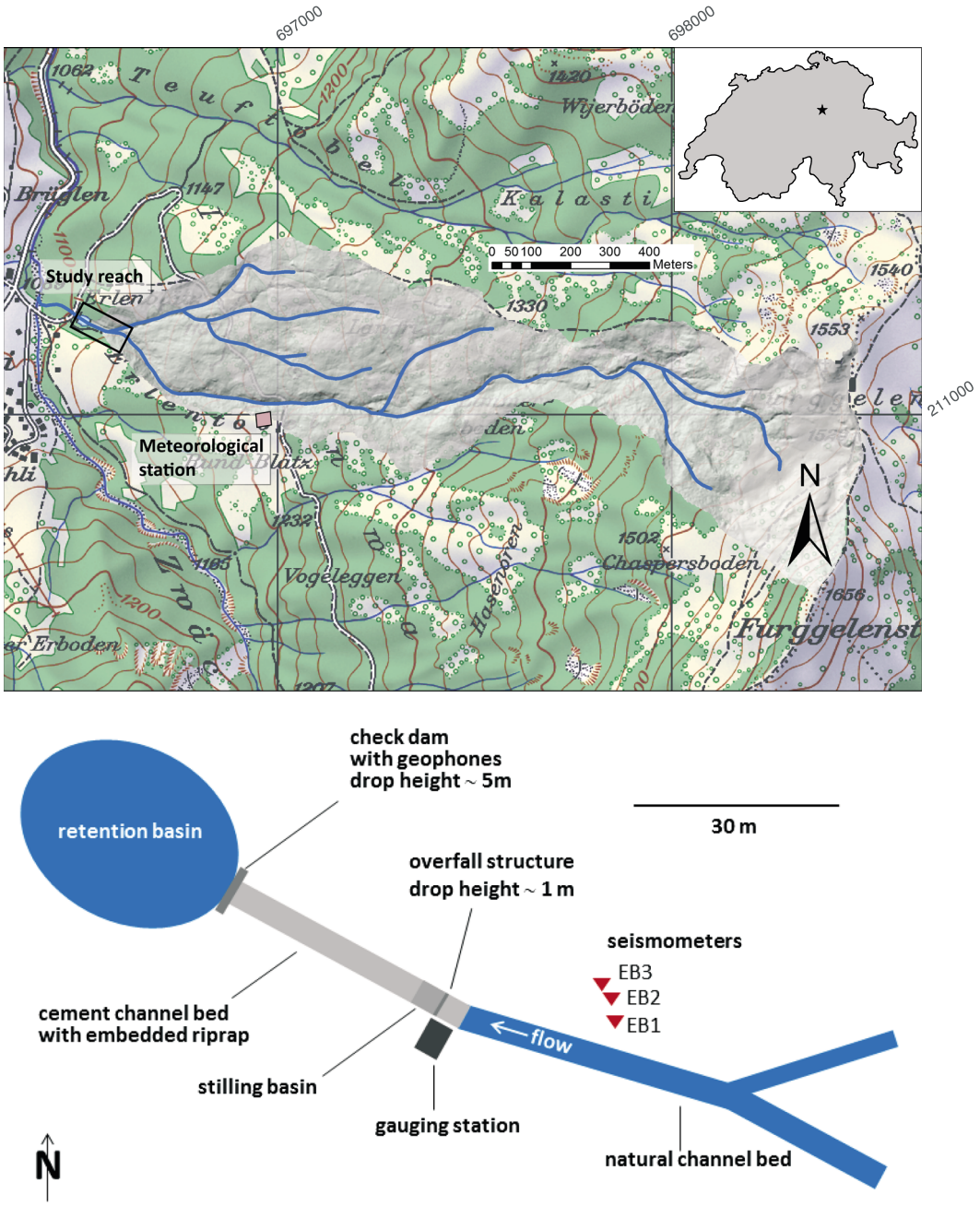

Figure 1. Maps of the Erlenbach in the Prealps in Switzerland (top right inset), as well as the study reach and channel network (top), and a schematic of the study reach and instrumentation (bottom).

we calculate 1 min average power spectral density (PSD) with Welch's averaging method [*Welch*, 1967] using 1 s windows with 50% overlap. We then sum the power over frequencies 35–55 Hz. Using different frequency bands between 1 and 100 Hz does not significantly alter the results of this analysis. The full spectrograms are available from *Roth et al.* [2016] along with a full analysis of the seismic spectra.

3. Hysteresis Metric Ψ

To calculate the amount of hysteresis in the relationship between water discharge and either seismic amplitude or geophone impulses during a given storm, we use a general nondimensional metric Ψ modified from *Roth et al.* [2014]:

$$\Psi = \frac{\sum_{Q_{min}}^{Q_{peak}} \left(y_{rise,Q} - y_{fall,Q} \right)}{\sum_{Q_{min}}^{Q_{peak}} \left(y_{rise,Q} + y_{fall,Q} \right)}, \quad (1)$$

where $y_{rise,Q}$ and $y_{fall,Q}$ are the relevant signal magnitude (in this case, seismic power or geophone impulses) at a given discharge Q on the rising and falling hydrograph limbs, respectively. Note that for a given discharge on a given limb multiple y -values may have occurred. In these cases, we take y_{rise} (y_{fall}) to be the average of all recorded y_{rise} (y_{fall}) values for that discharge. Moreover, the set of discharges recorded on the rising limb is not equal to the set of discharges recorded on the falling limb. We therefore cross interpolate y_{rise} and y_{fall} over the set of all measured discharge values for a given event to obtain a pair of y_{rise} and y_{fall} values for every discharge measured throughout the event. By summing the difference between the rising and falling limb amplitudes over the hydrograph from a selected minimum (Q_{min}) to peak (Q_{peak}) discharge, this metric measures the normalized area within the curve of seismic or geophone amplitude versus water discharge. The metric Ψ ranges in value between 1 and -1, where $\Psi > 0$ and $\Psi < 0$, respectively, indicate net clockwise and counterclockwise hysteresis. The end-member $\Psi = 1$ indicates $\sum y_{fall} = 0$ (i.e., all seismic power or sediment transport occurs on the rising limb), while $\Psi = -1$ indicates $\sum y_{rise} = 0$ (i.e., all seismic power or transport occurs on the falling limb).

It is important to note that the seismometers and geophones record different signals. For geophone hysteresis Ψ_G, the values in equation (1) are simply $y_{rise,Q} = g_{rise,Q}$ and $y_{fall,Q} = g_{fall,Q}$, or the rising and falling limb geophone impulse rates at discharge Q. However, the seismic power at any given point is the sum of seismic power generated by both bed load transport (B) and water turbulence (W). While there may be additional minor components contributing to the seismic signal, such as precipitation, we assume that they are negligible here for the sake of simplicity; this assumption is justified a posteriori in section 6.

The seismic hysteresis can therefore be further decomposed into

$$\Psi_S = \frac{\sum_{Q_{min}}^{Q_{peak}} \left(B_{rise,Q} - B_{fall,Q} + W_{rise,Q} - W_{fall,Q} \right)}{\sum_{Q_{min}}^{Q_{peak}} \left(B_{rise,Q} + B_{fall,Q} + W_{rise,Q} + W_{fall,Q} \right)}, \quad (2)$$

and, unlike Ψ_G, Ψ_S can never equal 1 or -1 in perennial streams since the signal of water turbulence W is always nonzero. This is the effect described by *Gimbert et al.* [2014], by which turbulence-induced seismic power modifies the hysteresis induced by sediment transport alone.

We use Q_{min} = 0.5 m^3/s to exclude data below the approximate threshold for grain detection by the geophones. *Roth et al.* [2016] observed that the impact of grains smaller than the geophones' technical recording threshold ($D \sim 10$ mm, mobile at $Q \sim 0.15$ m^3/s) may register on the seismometers [*Roth et al.*, 2016] and lead to some disagreement between seismometers and geophones at low transport rates. However, these small grains appear to make up a negligible portion of the total transport signal by the time the geophone transport rates reach ~100 imp/min [*Roth et al.*, 2016], which corresponds very roughly to ~0.5 m^3/s for the events in this study. The relatively small contribution of small grains to the seismic PSD at higher discharges reflects the fact that the signal of sediment transport is dominated by the largest mobile grains [*Tsai et al.*, 2012; *Turowski et al.*, 2015]. Hence, the signal of small grains is quickly drowned out as larger grains are mobilized. While varying Q_{min} between 0.15 m^3/s and 0.5 m^3/s can shift the exact values of either Ψ by up to 25%, it does not change the sign of Ψ_G or Ψ_S for any of the observed events; however, we use the more conservative threshold of 0.5 m^3/s to avoid any potential inconsistency.

Due to the low roughness on the Erlenbach's concrete-bed reach, sediment that enters this section is ultimately transported past the geophones by the end of each flood: essentially no sediment is retained on the engineered bed between transport events. Hence, we expect transport patterns recorded by the geophones to lag slightly behind patterns on the natural streambed near the seismic sensors ~60 m upstream. Because of the stochasticity of sediment transport processes, we also do not expect the short-term (i.e., minute-scale) transport patterns in the study reach to be accurately represented by the geophone recordings. While we consider the longer-term sediment transport rates to be more representative of the

transport along both the concrete-bed and study reaches, averaging over longer timescales decreases the resolution of the hydrograph peak, and hence the hysteresis in signals near the peak.

In order to maximize peak resolution and avoid mixing rising and falling limb hydrograph data, we process all data (discharge, seismic power, geophone impulses, and precipitation) using a moving mean with 9 min windows and 4 min overlap, centered on the time of peak discharge (in 1 min data) for each event. Nine minutes was selected to exceed the particle travel time between the seismometer and geophones, which was estimated as follows. For the range of discharges observed during our measuring campaign, the estimated flow velocity in the Erlenbach is ~0.6–1.4 m/s [*Nitsche et al.*, 2012] for the upper natural-bed reach (rough bed) from the seismometer to the overfall structure near the gauging station (Figure 1) (about 25 m) and roughly a constant ~5 m/s [*Wyss et al.*, 2016] for the lower concrete-bed reach (relatively smooth bed) from the end of the stilling basin to the geophone plates (~ 30 m). Assuming that sediment travels at ~20–40% and ~50–80% of the water velocity [e.g., *Julien and Bounvilay*, 2013], respectively, on rough (natural bed) and smooth (concrete bed) surfaces, then the total particle travel time between the seismometer and geophones is ~60–210 s or 2.6–9 times less than our 9 min averaging window.

Another potential cause of lag between transport rates at the seismometer and at the geophones is possible sediment storage in the shallow stilling basin itself, located under the overfall structure near the gauging station. The bed area there is roughly 4 m × 4 m; however, the engineered channel cross section above the overfall structure is slightly asymmetric with the thalweg against the southern bank (Figure 1), so only ~1/4–1/3 of the channel width and the stilling basin are active during events of the magnitude observed in this study. Assuming a maximum potential buffering (mean) sediment depth of about 0.1 m (from observations), this allows for a possible (temporary) storage volume of about 0.5 m^3. Using the linear relationship $IP = 3.27\,M$ between geophone impulses (IP) and sediment mass (M) in kilogram [*Rickenmann et al.*, 2012] and a bulk density of 1750 kg/m^3 [*Rickenmann and McArdell*, 2007], this maximum temporary storage would represent $\Delta IP = 2860$ imp. We estimate the maximum potential error this storage could generate in the geophone data by modeling two end-member scenarios: (a) all trapped sediment enters the stilling basin on the rising hydrograph limb and is released on the falling limb, such that the seismometer records its passage on the rising limb and the geophones record it on the falling limb (i.e., storage artificially shifts ΔIP from the rising limb to the falling limb). (b) Trapped sediment enters the stilling basin on the falling hydrograph limb and is not released until the rising limb of the next of the event, so the seismometers record the excess transport on the falling limb and the geophones record it on the rising limb (i.e., storage artificially moves ΔIP from the falling limb to the rising limb). We model the corrected Ψ_G with the sediment offset ΔIP in each of these scenarios being accommodated by either (i) a constant change in transport rate $\Delta g = \Delta IP/t_{\mathrm{rise/fall}}$ evenly distributed over the entire duration of the rising (t_{rise}) and/or falling (t_{fall}) limb (e.g., the time on each limb during which $Q_{\mathrm{min}} \le Q \le Q_{\mathrm{peak}}$) or (ii) a change in transport rate at a single point, $\Delta g = \Delta IP/t_{\mathrm{window}}$, where $t_{\mathrm{window}} = 9$ min is the length of the moving mean window:

$$\Psi_{G,\mathrm{corrected}} = \begin{cases} \dfrac{\sum_{Q_{\mathrm{min}}}^{Q_{\mathrm{peak}}}\left[\left(g_{\mathrm{rise},Q}\pm\dfrac{\Delta IP}{t_{\mathrm{rise}}}\right)-\left(g_{\mathrm{fall},Q}\mp\dfrac{\Delta IP}{t_{\mathrm{fall}}}\right)\right]}{\sum_{Q_{\mathrm{min}}}^{Q_{\mathrm{peak}}}\left[\left(g_{\mathrm{rise},Q}\pm\dfrac{\Delta IP}{t_{rise}}\right)+\left(g_{\mathrm{fall},Q}\mp\dfrac{\Delta IP}{t_{\mathrm{fall}}}\right)\right]} & \binom{a}{b},\mathrm{i}) \\ \dfrac{\sum_{Q_{\mathrm{min}}}^{Q_{\mathrm{peak}}}\left(g_{\mathrm{rise},Q}-g_{\mathrm{fall},Q}\right)\pm 2\dfrac{\Delta IP}{t_{\mathrm{fall}}}}{\sum_{Q_{\mathrm{min}}}^{Q_{\mathrm{peak}}}\left(g_{\mathrm{rise},Q}+g_{\mathrm{fall},Q}\right)} & \binom{a}{b},\mathrm{ii}) \end{cases} . \quad (3)$$

4. Results: Seismic Power and Hysteresis Do Not Scale as Expected With Sediment Transport Rates

We examine seismic and geophone data from five transport events in 2013, with peak discharges of 0.6–1.9 m^3/s. The discharge time series for each transport event is shown along with concurrent geophone impulse rate (linear with sediment transport), 35–55 Hz seismic power, and precipitation rate in

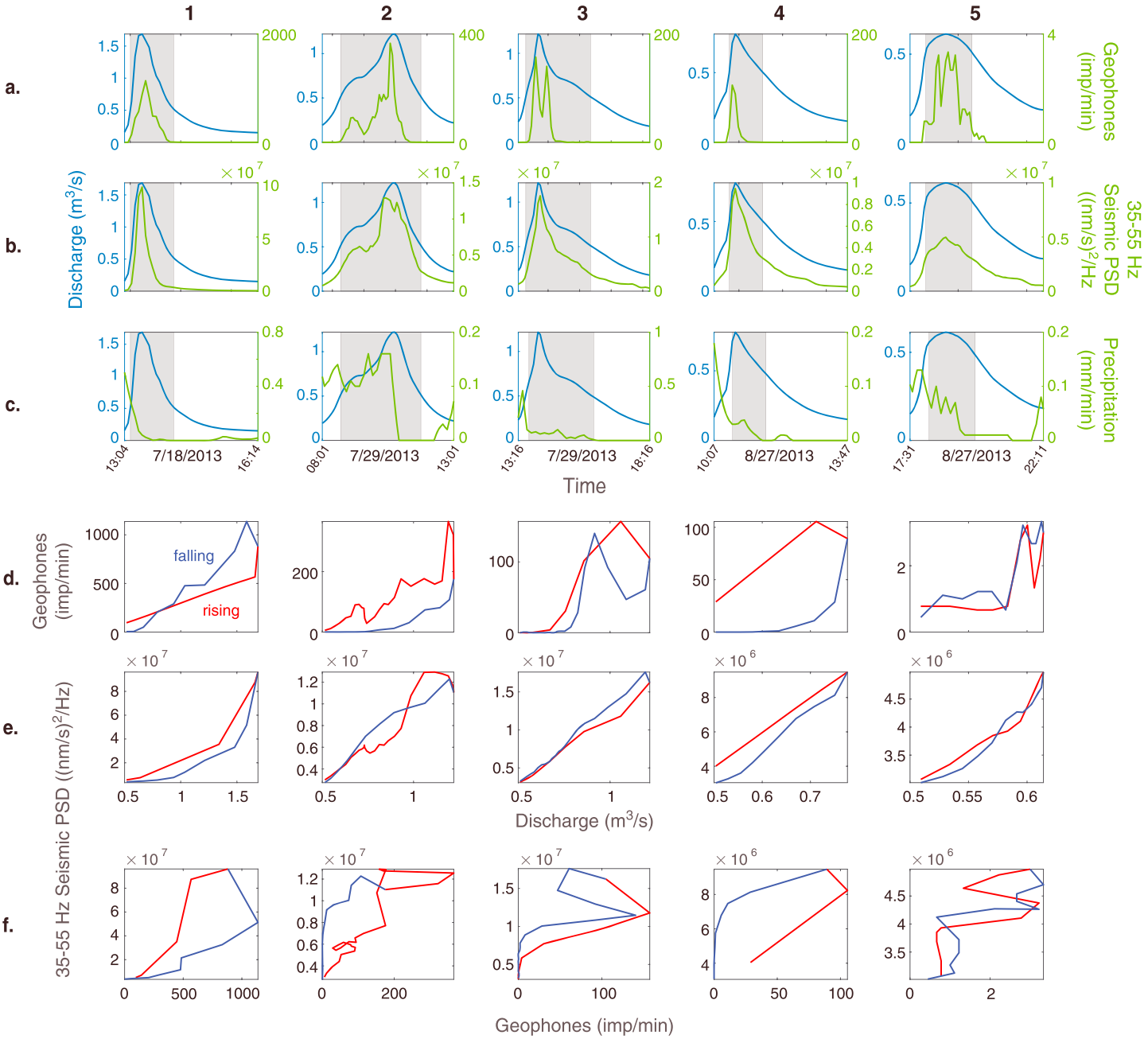

Figure 2. Time series of discharge for each transport event (1–5) with concurrent (a) geophone impulse rate (linear with sediment transport), (b) 35–55 Hz seismic power, and (c) precipitation rate; the gray boxes indicate range used for hysteresis analysis ($Q \geq 0.5$ m^3/s). Hysteresis in both (d) geophone impulse rate and (e) seismic power as a function of discharge, and (f) direct hysteresis between seismic power and geophone impulse rate. In all hysteresis loops, the red color indicates data on the rising limb, while the blue color indicates data on the falling limb.

Figures 2a–2c. Figures 2d and 2e show the hysteresis in both geophone impulse rate and seismic power as a function of discharge, and the direct hysteresis between seismic power and geophone impulse rate is shown in Figure 2f.

Our observations indicate that sediment transport does not generate the majority of seismic power recorded at this site. Under the simplifying assumption that no other seismic sources contribute noticeably to the signal, we can express a simple model for the dependence of seismic power P on sediment transport and discharge as $P \sim W + B$, where $W \sim \alpha Q^{1.25}$ [*Gimbert et al.*, 2014, 2016] is the theoretical seismic power generated by water turbulence, $B \sim \beta g$ [*Tsai et al.*, 2012] is the theoretical power

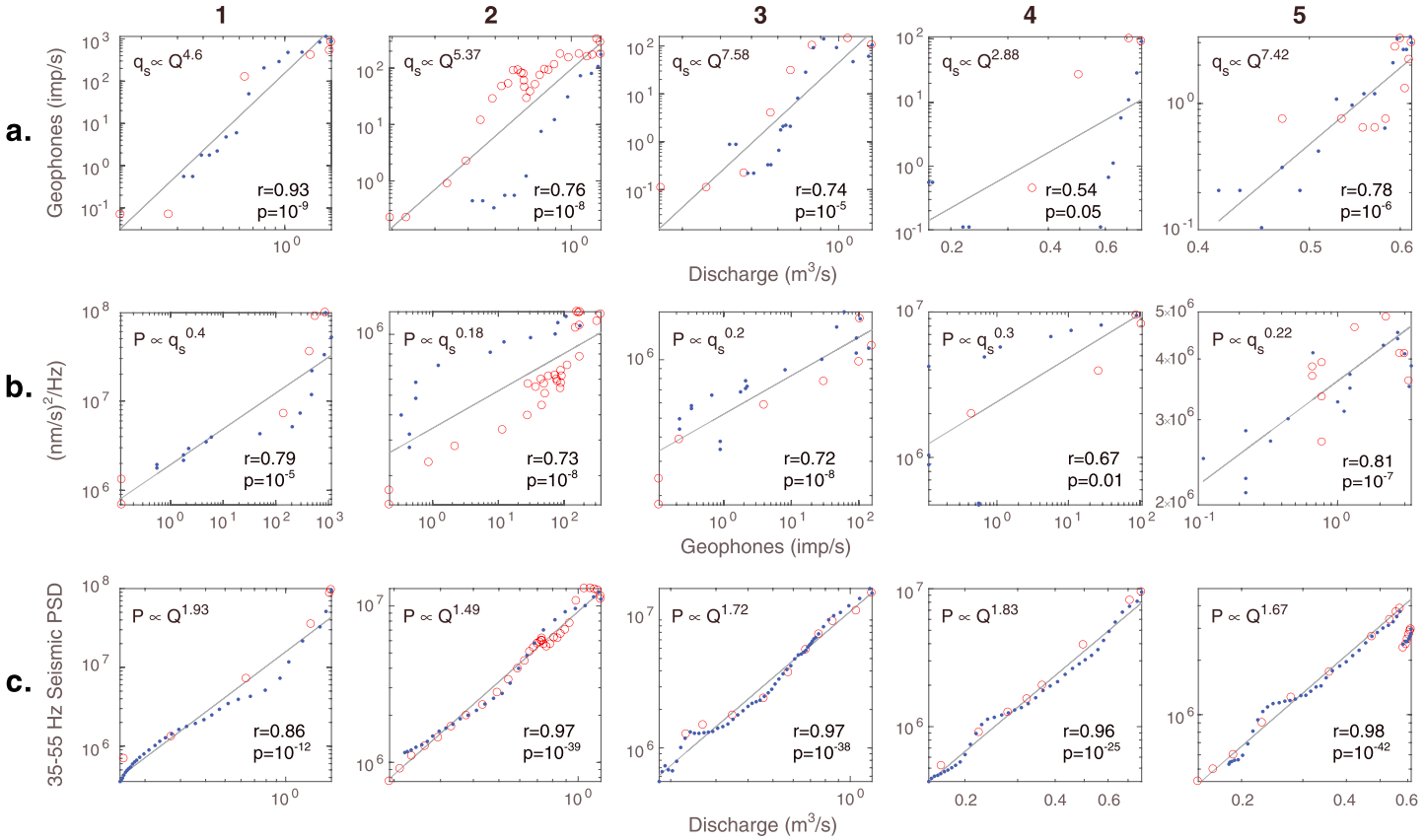

Figure 3. (a) Geophone impulses compared to concurrent discharge, and seismic power spectral density (PSD) as a function of (b) concurrent geophone impulses (sediment transport rate) and (c) discharge for each transport event (1–5). The gray lines and equations show regressions for each pair of variables and event; the red open circles and blue dots indicate rising and falling limb data, respectively. Theoretical and empirically calibrated relationships are $q_s \propto Q^5$ [*Hegg and Rickenmann*, 1999; *Rickenmann*, 2016], $P \propto q_s$ [*Tsai et al.*, 2012], and $P \propto Q^{1.25}$ [*Gimbert et al.*, 2014, 2016]. Regressions indicate that the seismic signal may be dominated by water turbulence rather than sediment transport.

generated by bed load (via its linear proxy, geophone impulse rate g), and α and β are scaling coefficients. Sediment flux has previously been shown to scale with discharge in the Erlenbach as $g \propto Q^5$ [*Hegg and Rickenmann*, 1999; *Rickenmann*, 2016], which is consistent with the range of exponents (2.88–7.58) obtained from power law regressions between geophone and discharge data (Figure 3a) for each of the five transport events observed in this study. Hence, we would expect seismic power to scale more closely to $P \propto g \propto Q^5$ if the seismic signal was dominated by bed load transport ($\alpha \geq \beta$), and more like $P \propto Q^{1.25} \propto g^{0.25}$ if water turbulence dominates the signal ($\alpha \ll \beta$) in the observed events. Regressions of the data show that $P \propto g^{0.18–0.4}$ (Figure 3b) and $P \propto Q^{1.49–1.93}$ (Figure 3c), only slightly higher than the theoretical scaling predicted for seismic power generated by discharge alone [*Gimbert et al.*, 2014, 2016]. This observation supports the postulation that water turbulence, rather than sediment transport, is the dominant source of seismic power at this site and is consistent with the results of *Turowski et al.* [2013b], who found that the energy transmitted to the geophones via bed load is small compared to the total energy of the water.

The hysteresis metric Ψ_S calculated from seismic data is shown as a function of the peak geophone impulse rate (a linear proxy for the peak sediment transport rate) for each storm in Figure 4. We do not find a statistically significant correlation ($r = 0.54$, $p = 0.3$) between these values, indicating that at this site, hysteresis in seismic power may not be an effective metric for the magnitude of sediment transport [e.g., *Roth et al.*, 2014]. We also find no statistically significant correlation ($r = -0.3$, $p = 0.6$) between the hysteresis metric calculated from seismic data (Ψ_S) and the same metric calculated from geophone data (Ψ_G) (error bars on Ψ_G from the maximum range of corrected values calculated in equation (3); Figure 5), indicating that a linear relationship may not always exist between the total observed seismic PSD and sediment

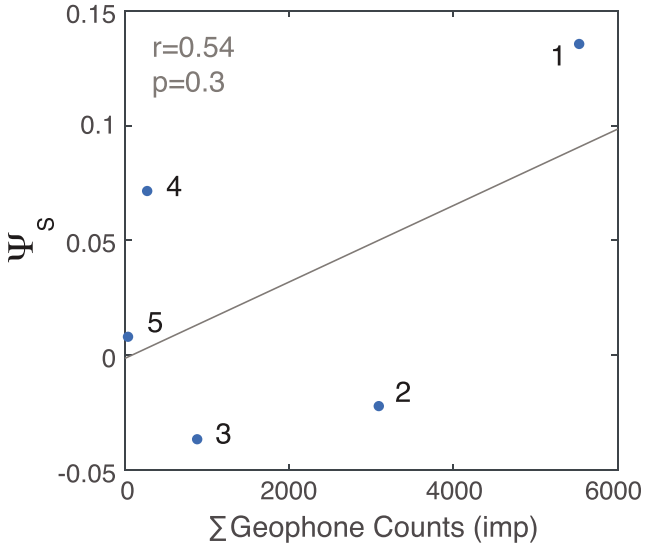

Figure 4. Hysteresis calculated from seismic data compared with total integrated geophone impulses (linear proxy for total sediment transport) over each transport event (1–5). We do not find statistically significant correlation between seismic hysteresis and sediment transport rates ($r = 0.54$, $p = 0.3$).

transport rates. More importantly, however, Ψ_S is also roughly an order of magnitude lower than Ψ_G, and we observe no consistent bias between Ψ_S and Ψ_G. In some events, the seismometer registered clockwise hysteresis and the geophones recorded counterclockwise hysteresis (events 1 and 5), whereas other events demonstrate the opposite pattern (events 2 and 3). This disagreement in the direction of hysteresis implies that the lack of correlation observed between seismic and geophone-derived hysteresis is not due to some systemic bias, such as the lag time hypothesized to exist between sediment transport patterns near the seismometer and at the geophones. Rather, this inconsistency points to one of two possibilities. First, the seismic signal of sediment transport may be generated or transmitted inconsistently over individual floods, perhaps due to evolution of the substrate material. Second, one or more processes in addition to bed load sediment transport may be contributing clockwise and/or counterclockwise hysteresis to the observed seismic signal. Such a process, or processes, would need to be highly nonlinear or stochastic to produce the variability in hysteresis observed between the seismic and geophone data.

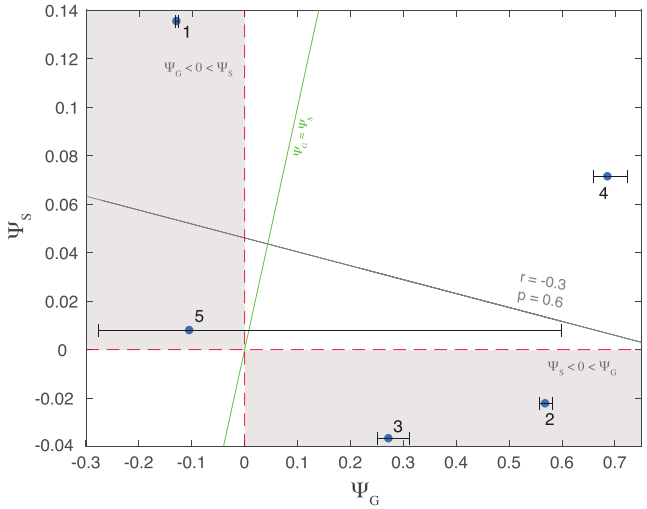

Figure 5. Hysteresis metric calculated from seismic (Ψ_S) and geophone (Ψ_G) data for each transport event (1–5). The red dashed lines are $\Psi_S = 0$ and $\Psi_G = 0$, and the gray regions demark areas where the direction of hysteresis is reversed between seismic and geophone data (clockwise versus counterclockwise). The green line indicates $\Psi_S = \Psi_G$, and the gray line shows regression between Ψ_S and Ψ_G ($r = -0.3$, $p = 0.6$). The error bars on Ψ_G represent the maximum range of values corrected for possible temporary sediment storage effects (equation (3)).

5. Possible Causes of Hysteresis

Numerous known processes may contribute to hysteresis either purely in sediment transport rates or in the seismic signal generated by water turbulence, or to both. These processes include changes in available sediment supply, evolution of transport efficiency and bed surface roughness due to changes in grain organization or sizes, and evolution of the turbulent flow velocity field due to the shifting of large boulders. Below we discuss these processes and the likelihood of them causing the observed disparity between geophone and seismic hysteresis.

5.1. Hysteresis in Sediment Transport

Exhaustion of sediment supply is a common cause of clockwise hysteresis in sediment transport over both individual floods and seasonal or annual timescales [e.g., *Nanson*, 1974; *Dunne*

and Leopold, 1978; *Reid et al.*, 1985; *Moog and Whiting*, 1998; *Whiting et al.*, 1999]. Similarly, counterclockwise hysteresis, while less frequently observed, has been found to be caused by increases in sediment supply, such as the arrival of a sediment pulse or sediment released from glacial melt [e.g., *Turowski et al.*, 2009; *Wulf et al.*, 2012; *Mao et al.*, 2014].

Hysteresis in sediment transport is also commonly ascribed to changes in transport efficiency due to bed evolution, such as coarsening or fining, armoring, and grain packing. When sediment supply is small relative to transport capacity, selective transport of small grains can progressively coarsen the bed, decreasing the number of exposed grains available for entrainment at a given stress [e.g., *Dietrich et al.*, 1989; *Wohl and Cenderelli*, 2000]. Progressive large-scale roughening of the bed can also be caused by the growth of bedforms such as ripples or dunes [*Martin and Jerolmack*, 2013]. If changes in discharge occur faster than the timescale for bed form adjustment [e.g., *Allen*, 1973; *Gee*, 1975; *Wijbenga and Klaassen*, 1983; *Baas*, 1994], then the evolution in bed form morphology will exhibit hysteresis by lagging behind changes in discharge [*Martin and Jerolmack*, 2013] This often leads to larger bedforms with higher friction for a given stage on the falling limb relative to the rising limb [e.g., *Allen*, 1974, 1976; *Ten Brinke et al.*, 1999; *Julien et al.*, 2002; *Wilbers and Ten Brinke*, 2003; *Frings and Kleinhans*, 2008; *Paarlberg et al.*, 2010], decreasing bed shear stress via form drag and causing transport efficiency to decline for a given stage on the falling limb of a flood event relative to the rising limb.

While the relationship between armor formation and hysteresis in individual storms is relatively undocumented, largely due to monitoring difficulties, numerous studies of gravel bed rivers have attributed clockwise hysteresis to the successive mobilization and reformation of bed armor on a flood's rising and falling limbs, respectively [e.g., *Kuhnle*, 1992; *Whiting et al.*, 1999; *Humphries et al.*, 2012]. To our knowledge, however, no clear mechanism for the implied asymmetry in armor destruction and formation processes is known. *Milhous and Klingeman* [1992] also linked counterclockwise hysteresis to the disturbance of a coarse surface armor, without subsequent reformation, which they proposed would make finer substrate available for transport thereafter.

Packing or restructuring of grains on the bed can progressively decrease grain mobility by increasing the bed shear stress required for entrainment [e.g., *Charru et al.*, 2004; *Mao*, 2012]. *Reid et al.* [1985] observed that consolidation of sediments in the channel bed over long periods between floods, or following low-magnitude floods, caused counterclockwise hysteresis in transport rates in subsequent events. Conversely, short periods following larger floods resulted in comparatively less consolidated sediment that was easily entrained on the next flood's rising limb, leading to clockwise hysteresis.

We do not have enough information about the state of the bed during floods to determine the extent to which any of these processes is actually responsible for the observed hysteresis in sediment transport. However, *Turowski et al.* [2011] examined floods in the Erlenbach from 1986 to 2009 and found a correlation between the critical discharges at which transport ceased in one event and started in the following event. They proposed that this was due to constant stochastic rearrangement of the bed during times with bed load transport, while in between floods, the bed does not change and is therefore stable. Further, the addition of fresh colluvial material may allow the bed to "reset" to some degree between storms and evolve again over each new hydrograph [e.g., *Turowski et al.*, 2011]. *Turowski et al.* [2009] also suggested that predominantly counterclockwise hysteresis during extreme flood events in the Erlenbach [*Turowski et al.*, 2009, 2013a] could be caused by the destruction of step-pool structures and subsequent release of finer material stored in the sediment wedges behind the steps. Sediment input from landslides [e.g., *Schuerch et al.*, 2006; *Golly et al.*, 2017] could also potentially influence hysteresis during extreme events larger than those observed during this study.

5.2. Effects of Boundary Conditions on Water Turbulence Signal and Hysteresis

As noted by both *Gimbert et al.* [2014] and *Roth et al.* [2014], while hysteresis in sediment transport rates may generate hysteresis in seismic amplitudes, the magnitude of the observed seismic hysteresis is modified by the addition of the signal generated by water turbulence. This effect is certainly present here because, as shown by *Roth et al.* [2016], the PSD of sediment transport and water turbulence overlap heavily in frequency and both peak between 35 and 55 Hz. This likely explains why the Ψ_S values are consistently about an order of magnitude lower than their Ψ_G counterparts, as the addition of the water turbulence signal "damps" any hysteresis present in the sediment transport signal. However, if the turbulence signal is constant for a given

discharge (i.e., $W_{rise,Q} = W_{fall,Q}$ in equation (2)), meaning that its contribution to the overall seismic amplitude is equal on the rising and falling limbs, then it can only damp the signal of sediment transport hysteresis Ψ_G (equation (2))—it cannot increase the magnitude or reverse the direction (i.e., clockwise to counterclockwise or vice versa) of total seismic hysteresis Ψ_S with respect to Ψ_G, as we see in our data (e.g., Figure 5, events 1, 2, 3, and 5). The observation that hysteresis in sediment transport rates (Ψ_G) and in seismic amplitudes (Ψ_S) can occur in opposing directions requires the presence of some amount of opposing hysteresis in either the turbulent flow signal or some other contributing source.

In fact, the occurrence of any of the bed evolution processes discussed above could also lead to some degree of hysteresis in the seismic signal generated by turbulent flow. Turbulent-flow-induced seismic power is expected to depend strongly on bed roughness and flow velocity [*Gimbert et al.*, 2014, 2016], which both influence the turbulent kinetic energy of the flow. Hysteresis in the water turbulence signal could therefore hypothetically be caused by changes in either (1) the grain-scale bed roughness exposed to the flow (e.g., due to bed coarsening/fining, armoring, or grain packing) or (2) macroroughness (e.g., due to bed form evolution, rearrangement of large structures/boulders, or changes in channel or bank geometry). *Gimbert et al.* [2014] predicts that although turbulence-induced seismic power is primarily set by river flow depth, slope, and width, there exists a secondary but significant contribution from the mean grain-scale bed roughness size; this scale controls both the drag exerted on the flow (and hence the average and turbulent flow velocities) [*Lamb et al.*, 2008], and the effective surface area over which fluid force fluctuations are applied to generate seismic waves. Although *Gimbert et al.* [2014] did not explicitly model the effects of macroscale roughness, similar reasoning can be applied to surmise the effects of roughness elements large enough to influence the flow velocity field and hydraulic geometry. Both grain-scale and larger-scale roughness changes would affect the average flow velocity and turbulence characteristics, but the latter would also affect the fluid shear velocities [e.g., *Wiberg and Smith*, 1991] contributing to the seismic signal [*Gimbert et al.*, 2014].

Below, we discuss in detail the ways in which bed evolution might cause the hysteresis we observe in seismic power on the Erlenbach. We assume that turbulent-flow-induced noise is the dominant source of this seismic power, as supported by the first-order power-discharge scaling regressions in our data (Figure 3, also see section 4), which roughly follow the theoretical predictions of *Gimbert et al.* [2014, 2016]. In section 5.2.2, we use the physical model of *Gimbert et al.* [2014] to provide a quantitative example that conceptually illustrates the effects of bed roughness and flow velocity on the seismic signal of water turbulence.

5.2.1. Plausible Causes of Hysteresis in Water Turbulence PSD

Because the seismic PSD generated by water turbulence is predicted to scale inversely with grain-scale bed roughness [*Gimbert et al.*, 2014], the observed change in the direction of hysteresis between the seismic and geophone data could not be explained by any bed evolution process that would also cause sediment transport rates to scale inversely with roughness, as these processes would work in tandem with and amplify the hysteresis caused by sediment transport. For example, while progressive coarsening of the bed may in fact occur, we would expect this to generate clockwise hysteresis in both sediment transport and the seismic PSD of water turbulence. However, bed evolution could still cause the hysteresis observed in the turbulence PSD by changing the bed roughness or flow velocity in a manner that does not generate correlated hysteresis in sediment transport, as follows.

A key way that roughness is often modified in the Erlenbach is through erosion and deposition of sediment surrounding large, essentially immobile boulders. One can identify two distinct transport thresholds for step-pool channels like the Erlenbach [*Montgomery and Buffington*, 1997]. During frequent storms, gravel moves through, over and around the steps. However, only very infrequently do storms of sufficient magnitude occur to directly mobilize the steps themselves. Indeed, on the Erlenbach only four flows of this magnitude have occurred in past >35 years of monitoring [*Turowski et al.*, 2009, 2013a], although shifting, slumping, or toppling of boulders can occur due to downstream scouring during lower flows [*Crowe*, 2002; *Church and Zimmermann*, 2007]. Hence, much of the flow's boundary shear stress acts on the essentially immobile boulders and not on the gravel on the bed [*Wiberg and Smith*, 1991; *Yager et al.*, 2007, 2012a]. Because channel hydraulics are highly sensitive to the degree of boulder protrusion above the gravel bed [*Yager et al.*, 2007], modifications to the manner in which flow interacts with the boulders due to changes in gravel deposition or shifting of boulders could change the local turbulent eddy field and boundary macroroughness such that changes in transport rates and changes in the turbulent-flow-induced seismic power are uncorrelated.

Figure 6. Small rock jam (indicated by red arrow) that formed during transport event 1, cutting off a small cascade between two large, immobile boulders and replacing it with a turbulent stall instead.

For example, an increase in boulder drag (counterclockwise seismic hysteresis) would also decrease the fluid shear stress available for sediment transport (clockwise transport hysteresis).

Changes in the dimensions of the spaces around, between and even, in some cases, beneath large boulders due to rearrangement of surrounding grains or minor shifting of the boulders via downstream scour could also substantially alter the turbulent eddy and flow velocity fields based on the way flow interacts with these constrictions and protrusions. When combined with the inhomogeneity of the channel bed and the proximity of the seismometer, minor changes in flow have the potential to significantly impact the seismic signal. For example, the small rock jam shown in Figure 6 formed at some point during transport event 1 and effectively cut off the flow that had previously cascaded between two large boulders and over a third large boulder at their base, shifting the flow to a gravel bedded section farther from the seismometer and replacing the boulder-coupled cascade with a turbulent stall. While we lack further documentation of bed rearrangement during this study period, previous studies on the Erlenbach have shown that substantial changes in bed configuration, roughness, and boulder protrusion occur frequently and at the event scale [*Turowski et al.*, 2011; *Yager et al.*, 2012a, 2012b]. Since the turbulent flow signal scales strongly with shear velocity $\left(P \propto u_*^{14/3}\right)$ [*Gimbert et al.*, 2014], small changes in velocity have the potential to drastically influence the seismic power. We expect the seismic PSD generated by highly turbulent flows such as cascades, for example, to be particularly sensitive to such shifting, as a larger proportion of the total flow is constrained to the pathways between and around boulders.

Similarly, some seismic hysteresis could occur due to shifting of grains at the base of the waterfalls into the shallow stilling basin (~25 m away, ~1 m drop) and retention basin (~60 m away, ~ 5 m drop) downstream of the study reach, which *Roth et al.* [2016] found may contribute strongly to the signal of water turbulence at this site. Since waterfalls are coupled to the ground via the bed at their bases, any rearrangement of grains here could significantly alter the seismic signal at a given discharge. In this specific case, both waterfalls are engineered, so grain rearrangement at the base is in fact the only way for the observed hysteresis to occur. Progressive filling of the lower retention basin with water could also generate some hysteresis but could only explain hysteresis in one direction (clockwise or counterclockwise). Hence, this explanation is simply another potential iteration of seismic hysteresis being induced by changing boundary conditions at the bed.

Also worth noting is that any evolution of the bed could also change the coupling between the water and the bed (i.e., the seismic transfer function) as well as transmission of energy through the bed (i.e., anelastic attenuation or seismic quality factor), either by altering the bed itself [e.g., *Kean et al.*, 2015] or by redirecting portions of the flow to different regions. The example shown in Figure 6 and discussed above, for instance, altered the source-receiver distance, the substrate through which the flow was coupled to the bed (large boulder versus gravel) and the path along which seismic waves were transmitted through the bed. However, the degree to which these changes might alter the relationship between discharge and the seismic PSD has not yet been quantitatively examined. Changes in river bank geometry could also affect the propagation of seismic waves, although we do not expect this to factor significantly into the hysteresis observed here as the banks of the study reach are partially engineered with large boulders that were not observed to move during the study period. Other ground site properties, such as soil saturation, could also influence wave propagation. However, because waves traveled comparatively longer distances through the channel bed than the bank (the seismometer was located only ~1 m from the edge of the ~5 m wide channel) and

large-scale changes in ground site properties (i.e., gravel rearrangement) are known to have occurred in the bed, it seems likely that any changes in seismic wave propagation would be predominantly due to changes in the bed rather than the banks. Changes in wave propagation due to ground saturation could also generate hysteresis in only one direction, as the ground becomes increasingly saturated over the course of each storm event, and thus could not explain the seismic hysteresis observed in all events.

Hence, we offer as a plausible explanation that shifting or rearrangement of grains may alter the seismic signal generated by fluid flow in two ways: first, by changing the turbulent intensity and kinetic energy of the flow via changes or excursions in hydraulic parameters via boundary conditions (e.g., bed roughness) and second, by changing the seismic transmission of turbulent energy to and through the bed. In either case, the proposed forms of bed evolution on the Erlenbach, either around large boulders or at the base of the waterfalls, would not need to correlate with the changes in sediment transport rate recorded by the geophones and could explain why the discrepancy between the seismic and geophone hysteresis appears to be so stochastic.

5.2.2. Theoretical Effects of Bed Roughness and Flow Velocity on Seismic Power

While it is still unknown how changes in large excursions in macroroughness or in the heterogeneity of flow velocities such as those that may have occurred on the Erlenbach might quantitatively influence the seismic signal of water turbulence, the model developed by *Gimbert et al.* [2014] provides us with a simple, first-order appraisal of the effects of changes in mean grain-scale bed roughness and fluid shear velocity. We use this model below to provide a quantitative illustration of the capacity for these mean properties to significantly influence the seismic signal but emphasize that this does not necessarily translate into an interpretation of our data, as the impact of excursions on both the turbulence power and sediment transport rates may differ significantly. It is also worth noting that this model accounts for isolated changes in mean grain-scale bed roughness and shear velocity and does not address the effects of bed roughness elements large enough to influence channel hydraulics and hence shear velocity (via flow depth).

The total seismic PSD (W) of ground motion per unit grain size due to water turbulence depends on the mean grain-scale bed surface roughness k_s and mean fluid shear velocity u_* through the functions

$$W(f;D) \propto k_s^{-2/3} p(D) D^2 \zeta(H/k_s) u_*^{14/3} \chi(f;D)^2, \tag{4}$$

(from equations (32) and (42) of *Gimbert et al.* [2014]), where $p(D)$ (m^{-1}) is the log-"raised cosine" distribution of grain size D [*Tsai et al.*, 2012], which depends on the median grain size $D_{50} = k_s/3$ [*Gimbert et al.*, 2014]. The function

$$\zeta(H;k_s) \propto \left[\left(1 - \left(\frac{k_s}{2H}\right)\right)^{1/3} \left(1 - \left(\frac{k_s}{4H}\right)\right)^{4/3} \left(5.62 \log_{10}\left(\frac{H}{k_s}\right) + 4\right)^{2/3} \right]^2 \tag{5}$$

[*Gimbert et al.*, 2014, equation 33] depends on flow depth H relative to bed roughness and accounts for modulations in seismic power due to variations in turbulent intensity and flow velocity within the bed roughness [*Gimbert et al.*, 2014, equation 33]. The function

$$\chi(f;D) = \frac{1}{1 + \left[\frac{2f}{f_c(D)}\right]^{4/3}} \tag{6}$$

[*Gimbert et al.*, 2014, equation 28] describes the capacity for grains of size D to convert flow velocity fluctuations into force fluctuations at frequency f (i.e., the transfer function between fluid velocity spectrum and pressure spectrum) [*Gimbert et al.*, 2014, equation 28]. At frequencies higher than the cutoff frequency

$$f_c(D) \equiv \frac{u_*}{0.12D}\left(1 - \left(\frac{k_s}{4H}\right)\right), \tag{7}$$

χ decreases because local force fluctuations cancel each other out.

We illustrate the potential effects of changes in mean grain-scale bed roughness and shear velocity on water turbulence seismic power in Figure 7. Figure 7a shows the theoretical ratio of falling to rising limb seismic power W_{fall}/W_{rise} calculated from equation (4) as a function of the fractional change in shear velocity on the falling and rising limbs, $u_{*,fall}/u_{*,rise}$, assuming all other variables remain constant. Similarly, Figure 7b shows the ratio W_{fall}/W_{rise} as an isolated function of the fractional change in rising and falling limb mean

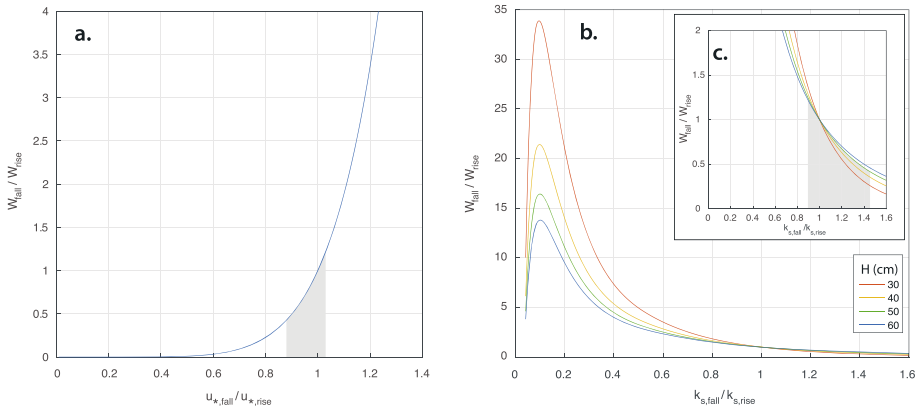

Figure 7. Theorized fractional change in the seismic PSD W generated by water turbulence on rising and falling hydrograph limbs, as a function of the fractional change in (a) fluid shear velocity u_* [*Gimbert et al.*, 2014, equations 41 and 43] (fixed $u_{*,\mathrm{rise}}$ = 1 m/s and k_s = 0.24 m) and (b) mean bed roughness k_s (fixed $k_{s,rise}$ = 0.24 m and u_* = 1 m/s) at different flow depths H [*Gimbert et al.*, 2014, equations 32 and 33], with inset (c) showing close-up of relevant values for observed transport events. The gray regions show $k_{s,\mathrm{fall}}/k_{s,\mathrm{rise}}$ and $u_{*,\mathrm{fall}}/u_{*,\mathrm{rise}}$ range associated with observed hysteresis ($0.4 \leq P_{\mathrm{fall}}/P_{\mathrm{rise}} \leq 1.2$).

bed roughness, $k_{s,\mathrm{rise}}$ and $k_{s,fall}$ (calculated from *Gimbert et al.*, 2014]), where the rising limb roughness is set to $3D_{50}$ [e.g., *Gimbert et al.*, 2014] or $k_{s,\mathrm{rise}}$ = 0.24 m and frequency and grain size have both been summed over 35–55 Hz and 0–0.10 m, respectively. Flow depth is shown for $0.3 < H < 0.6$ m, corresponding to discharges between ~0.3 and 1.9 m^3/s (from the calibrated stage-discharge relationship for the Erlenbach [e.g., *Beer et al.*, 2015]). Above $k_{s,\mathrm{fall}}/k_{s,rise} \sim 0.1$, the turbulence force decreases with increasing bed roughness because rougher beds exert more friction on the flow, decreasing the average flow velocity and turbulence intensity (i.e., the root-mean-square of the fluctuating streamwise velocities) [*Lamb et al.*, 2008]. Conversely, relatively much smoother beds ($k_{s,\mathrm{fall}}/k_{s,\mathrm{rise}} \lesssim 0.1$) have less specific area exposed to the flow, and thus turbulent flow forces decrease with decreasing roughness. As noted by *Gimbert et al.* [2014], we also see that the dependence on roughness increases with relative roughness k_s/H. Hence, we expect mean roughness to strongly influence seismic power in rivers where flow depth is shallow with respect to the scale of mean bed roughness, as it is on the Erlenbach; for rivers with relatively deeper flow depths, we expect the seismic signal of water turbulence to be less sensitive to the boundary conditions at the bed.

We can perform a simple scaling analysis on our seismic data to demonstrate the approximate changes in mean roughness or mean shear velocity that would be required to generate the observed hysteresis. Again, we emphasize that this example is intended to be conceptually illustrative but does not necessarily represent the effects of changes in roughness and velocity excursions that may actually have occurred. For this simple demonstration, we assume the entire difference in hysteresis between the seismic and geophone data is caused by changes in the seismic signal generated by water turbulence and that the changes in water turbulence are entirely generated by isolated changes in either mean grain-scale bed roughness or shear velocity (ignoring any conflicting hysteresis this might also cause in sediment transport rates). We then estimate the change in mean bed roughness or shear velocity on the rising and falling limbs, $k_{s,\mathrm{rise}}$ and $k_{s,\mathrm{fall}}$ or $u_{*,\mathrm{rise}}$ and $u_{*,\mathrm{fall}}$, respectively, needed to independently produce the ratio of rising and falling limb total seismic power, $P_{\mathrm{fall}}/P_{\mathrm{rise}}$ (where $P \sim W + B$ as in equation (2) and section 4) for two end-members of the observed transport events: 1 and 3. In transport event 1, for example, the seismic hysteresis is clockwise and the geophone hysteresis is counterclockwise. We therefore assume that the water turbulence signal experienced clockwise hysteresis large enough to cancel out the counterclockwise hysteresis generated by sediment transport (which may already have been significantly damped simply by the addition of the turbulence signal) and to add on additional clockwise hysteresis in the total seismic signal. Hence, we treat the full magnitude of observed seismic hysteresis as a lower bound on the hysteresis generated by fluid flow, such that the ratio of the rising and falling limb seismic power $W_{\mathrm{fall}}/W_{\mathrm{rise}} \leq P_{\mathrm{fall}}/P_{\mathrm{rise}}$ for $P_{\mathrm{fall}}/P_{\mathrm{rise}} < 1$ (e.g., event 1) and $W_{\mathrm{fall}}/W_{\mathrm{rise}} \geq P_{\mathrm{fall}}/P_{\mathrm{rise}}$ for $P_{\mathrm{fall}}/P_{\mathrm{rise}} > 1$ (e.g., event 3).

In transport event 1, the minimum ratio of falling to rising limb seismic power provides an upper limit of $W_{fall}/W_{rise} \leq P_{fall}/P_{rise} \sim 0.4$ (clockwise) (Figure 2e) at $H \sim 0.47$ m ($Q \sim 0.9$ m^3/s). Conversely, in transport event 3 we observe a maximum increase in seismic power $W_{fall}/W_{rise} \geq P_{fall}/P_{rise} \sim 1.2$ (counterclockwise) at $H \sim 0.5$ m ($Q \sim 1.1$ m^3/s). Generating these changes in seismic power would require fractional changes in fluid shear velocity of $u_{*,fall}/u_{*,rise} \lesssim 0.87$ (event 1) and $\gtrsim 1.03$ (event 3) (Figure 7a) or a roughly 3–13% change. Alternately, the change in seismic power could be produced by a change in mean bed roughness of $k_{s,fall}/k_{s,rise} \gtrsim 1.45$ (event 1) and $\lesssim 0.9$ (event 3) (Figure 7b). If these changes in roughness are proportional to changes in median grain size on the bed ($k_s \sim 3D_{50}$), then the change in seismic amplitudes over these transport events would correspond to a minimum change from $D_{50} \sim 80$ mm on the rising limb to ~116 mm (event 1) or ~72 mm (event 3) on the falling limb. While changes in median grain size have not been studied systematically on the Erlenbach, these numbers may be reasonable [e.g., *Parker*, 1990; *Wilcock and McArdell*, 1997] as roughness is known to evolve here due to winnowing following extreme events that reset the median grain size [e.g., *Yager et al.*, 2012b].

The simplified, first-order calculations presented here highlight the seismic signal's sensitivity to hydraulic parameters, especially in relatively rough and shallow streams like the Erlenbach. As previously noted, however, these calculations only describe the effects of mean bed roughness and shear velocity on the seismic PSD, whereas the shifts in grain arrangement or boulder position we suggest would generate velocity and roughness excursions not currently addressed by the model [*Gimbert et al.*, 2014]. Future work can help to better address the effects of these large excursions, which may play a large role in the seismic signal generated by turbulent flow in steep mountain streams, cascades, and other similar settings. Similarly, additional research could help constrain the extent to which bed structure, which can vary and evolve drastically in such settings, may influence the seismic transfer function and quality factor.

6. Discussion and Conclusions

We use a normalized metric to compare the hysteresis in 35–55 Hz band-averaged seismic power spectral density and geophone impulse rates (a linear proxy for coarse sediment transport rates) as functions of flood discharge over five transport events on the Erlenbach stream in the Swiss Prealps. We find that seismic power more closely follows the predicted scaling with water discharge than with sediment transport and that hysteresis in seismic power is roughly an order of magnitude lower than hysteresis in transport rates. This implies that water turbulence, rather than coarse sediment transport, may dominate the seismic signal for the investigated range of flow and bed load transport conditions. We see no significant correlation between seismic hysteresis and sediment transport ($r = 0.54$, $p = 0.3$), indicating that for small to moderate events in this location, seismic hysteresis may not be a reliable qualitative indicator of the presence or magnitude of sediment transport. We also fail to find significant correlation between the magnitudes of hysteresis in seismic power and in sediment transport rates ($r = -0.3$, $p = 0.6$), which occur in opposing directions (clockwise versus counterclockwise) in 4 out of the 5 hydrograph events recorded in this study. These results refute the commonly held assumption that seismic hysteresis reflects changes in the rate of coarse sediment transport.

We suggest that changes in the water turbulence signal provide a plausible alternative mechanism for the hysteresis observed in the seismic signal, possibly due to evolving boundary conditions at the bed (i.e., shifting or rearrangement of sediment). Shifting or rearrangement of grains could cause hysteresis in the seismic signal of fluid flow either (i) by changing the turbulent kinetic energy of the flow at a given discharge or (ii) by changing the coupling between the fluid flow and bed continuum.

The accumulation of loose sediment on the channel bed from the surrounding hillsides enables the bed to constantly evolve and then "reset" to some extent between storms. While the exact nature of bed evolution occurring at this site is not known, the reversed directions of seismic and geophone hysteresis cannot be explained by any process that causes positively correlated hysteresis in sediment transport and the water turbulence signal, such as progressive roughening of the bed. Hence, we suggest that hysteresis in the fluid flow-generated signal could potentially be explained by stochastic changes in the bed roughness and/or in the flow velocity field due to rearrangement of grains around and between large boulders, or at the base of a downstream waterfall. Minor shifting of these highly angular boulders due to downstream scour could also alter the turbulent flow around them, leading to hysteresis in local flow velocity. The seismic signal generated by fluid flow is highly sensitive to minor shifts in boundary conditions at the bed, and relatively

modest changes in the mean, grain-scale bed roughness (±30%) or shear velocity (±15%) could theoretically yield turbulence-generated seismic hysteresis on the scale of the observed discrepancy between the geophone and seismic data. However, these estimates do not necessarily represent the effects of large velocity excursions and changes in macroscale roughness that could be caused by bed reorganization.

Other sources of hysteresis in the seismic signal could include rainfall and a downstream pressure gradient on the falling limb [*Hsu et al.*, 2011], both of which, however, are implausible explanations for the discrepancy between seismic and sediment transport hysteresis. If heavy rainfall were to occur on either limb of the hydrograph, it could add some amount of hysteresis to the seismic signal between 35 and 55 Hz [*Roth et al.*, 2016]. However, we can rule out rainfall as the primary cause of disagreement between the seismic and geophone data because precipitation data (Figure 2c) shows that it occurs primarily on the rising hydrograph limb of all the transport events. Hence, rainfall could not be the source of the excess counterclockwise hysteresis in transport events 2 and 3. Similarly, contrast between the downstream pressure gradient generated by the rising limb flood wave and the upstream pressure gradient on the falling limb [*Hsu et al.*, 2011] could theoretically generate some clockwise but not counterclockwise hysteresis. Other seismic sources such as wind shaking trees, wildlife, or anthropogenic noise are possible and may contribute some hysteresis to the signal.

Our results have significant implications for the growing field of fluvial seismology, as most studies have previously construed seismic hysteresis as evidence both for sediment transport as a main source of seismic noise and for hysteresis in sediment transport. Our results demonstrate that these interpretations may not always be valid because the coupling between sediment transport and changes in hydraulic parameters is more complex than previously expected. By changing the shape of the boundary over which water flows, bed evolution fundamentally influences the fluid dynamical parameters that control water turbulence. Hence, our findings highlight the possibility that although seismic hysteresis may be correlated with transport in some settings, this hysteresis may be caused by changes in water turbulence due to evolution of the bed, rather than actual changes in the rate of sediment transport. This may be especially true in rivers where flow depth is low or comparable to the largest roughness elements on the bed or where highly turbulent features such as waterfalls or cascades may contribute significantly to the seismic signal. For instance, it seems likely that the correlation found by *Roth et al.* [2014] between sediment transport rates and seismic hysteresis on the Chijiawan—another relatively rough and shallow river—in Taiwan may also have reflected changes in the water turbulence signal due to the large-scale evolution of the bed surface. Seismic hysteresis reported in other rivers where cascades are present or bed evolution is thought to have occurred [e.g., *Hsu et al.*, 2011; *Schmandt et al.*, 2013; *Barrière et al.*, 2015] could also be at least partially caused by subsequent changes in the fluid-generated signal. Quantitative interpretations based on hysteresis in seismic signals, in particular, may also overestimate or underestimate changes in bed load transport since the addition of the water turbulence signal, as well as any hysteresis in the turbulence signal caused by bed evolution, could obscure these estimates. For example, *Schmandt et al.* [2013] estimated that following the model of *Tsai et al.* [2012], their observed hysteresis could correspond to bed load flux changing by factors of roughly 2.5–3.2 and 8, while *Hsu et al.* [2011] suggested that hysteresis in their data could imply a roughly twofold decrease in transport efficiency. Since bed evolution can only occur if sediment has moved, hysteresis in water turbulence-induced seismic power may still indicate the presence of some amount of transport and be qualitatively useful for learning about transport under certain conditions, such as when bed roughness is relatively small with respect to flow depth. More research is needed to further constrain these conditions, as well as the effects of large velocity and roughness excursions on fluid flow-generated seismic signals, the relationship between bed roughness and flow velocity in the turbulence-generated seismic power model, and the extent to which changes in bed solely on hysteresis structure and other ground site properties can influence the propagation of seismic waves. Better understanding of these factors would help determine the extent to which seismic hysteresis may relate to sediment transport rates in different fluvial settings and may improve our ability to quantitatively interpret hysteresis in seismic signals near rivers.

However, our results also point to the need for future work to move beyond relying solely on hysteresis by focusing on developing more quantitative methods to isolate the sources contributing to seismic signals. For example, *Roth et al.* [2016] did not rely on the observation of hysteresis, but rather used independently constrained bed load transport, discharge, and precipitation data to identify the seismic spectra generated by each process. Such approaches calibrated with real data or utilizing seismic spectral decomposition may prove more effective than those that use hysteresis alone.

Acknowledgments
We thank John Buffington, Amy East, Rebecca Hodge, and two anonymous reviewers for helping to evaluate and improve this manuscript, and we gratefully acknowledge the contributions and assistance of Claire Masteller, Alex Beer, Johannes Schneider, Carlos Wyss, Claudia Bieler, Nicolas Zogg, Bruno Fritschi, Jon Perkins, Leonard Sklar, Jim Kirchner, Thorne Lay, Daniel Sampson, Ed Boring, Heather Deshon, Rob Laber, Mikael Witte, Kerri Johnson, Alex Nereson, Allison Pfeiffer, and David Santaniello. We are also grateful for the support of Pnina Miller, Noel Barstow, George Slad, Jackie Gonzales, Mouse Reusch, Katherine Anderson, and other members of the PASSCAL Data, Training, and Logistics Groups. This work was supported by NSF Geomorphology and Land Use Dynamics grant EAR 1148488. The seismic instruments used in this study were provided by the Incorporated Research Institutions for Seismology (IRIS) through the PASSCAL Instrument Center at New Mexico Tech. Seismic data collected will be available through the IRIS Data Management Center. The facilities of the IRIS Consortium are supported by the National Science Foundation under cooperative agreement EAR-1261681 and the DOE National Nuclear Security Administration.

References

Allen, J. (1973), Phase differences between bed configuration and flow in natural environments, and their geological relevance, *Sedimentology*, *20*(2), 323–329, doi:10.1111/j.1365-3091.1973.tb02054.x.

Allen, J. (1974), Reaction, relaxation and lag in natural sedimentary systems: General principles, examples and lessons, *Earth-Sci. Rev.*, *10*(4), 263–342, doi:10.1016/0012-8252(74)90109-3.

Allen, J. (1976), Time-lag of dunes in unsteady flows: An analysis of Nasner's data from the R. Weser, Germany, *Sediment Geol.*, *15*(4), 309–321, doi:10.1016/0012-8252(74)90109-3.

Baas, J. H. (1994), A flume study on the development and equilibrium morphology of current ripples in very fine sand, *Sedimentology*, *41*(2), 185–209, doi:10.1111/j.1365-3091.1994.tb01400.x.

Barrière, J., A. Oth, R. Hostache, and A. Krein (2015), Bed load transport monitoring using seismic observations in a low-gradient rural gravel bed stream, *Geophys. Res. Lett.*, *42*, 2294–2301, doi:10.1002/2015GL063630.

Beer, A. R., J. M. Turowski, B. Fritschi, and D. H. Rieke-Zapp (2015), Field instrumentation for high-resolution parallel monitoring of bedrock erosion and bedload transport, *Earth Surf. Process. Landf.*, *40*(4), 530–541, doi:10.1002/esp.3652.

Burtin, A., L. Bollinger, J. Vergne, and J. L. Nábelek (2008), Spectral analysis of seismic noise induced by rivers: A new tool to monitor spatiotemporal changes in stream hydrodynamics, *J. Geophys. Res.*, *113*, B05301, doi:10.1029/2007JB005034.

Burtin, A., J. Vergne, L. Rivera, and P. Dubernet (2010), Location of river-induced seismic signal from noise correlation functions, *Geophys. J. Int.*, *182*(3), 1161–1173, doi:10.1111/j.1365-246X.2010.04701.x.

Burtin, A., R. Cattin, L. Bollinger, J. Vergne, P. Steer, A. Robert, N. Findling, and C. Tiberi (2011), Towards the hydrologic and bed load monitoring from high-frequency seismic noise in a braided river: The "Torrent de St Pierre", French Alps, *J. Hydraul.*, *408*(1), 43–53, doi:10.1016/j.jhydrol.2011.07.014.

Burtin, A., N. Hovius, and J. M. Turowski (2016), Seismic monitoring of torrential and fluvial processes, *Earth Surf. Dyn.*, *4*(2), 285, doi:10.5194/esurf-4-285-2016.

Chao, W. A., Y. M. Wu, L. Zhao, V. C. Tsai, and C. H. Chen (2015), Seismologically determined bedload flux during the typhoon season, *Sci. Rep.*, *5*, 8261, doi:10.1038/srep08261.

Charru, F., H. Mouilleron, and O. Eiff (2004), Erosion and deposition of particles on a bed sheared by a viscous flow, *J. Fluid Mech.*, *519*, 55–80, doi:10.1017/S0022112004001028.

Church, M., and A. Zimmermann (2007), Form and stability of step-pool channels: Research progress, *Water Resour. Res.*, *43*, W03415, doi:10.1029/2006WR005037.

Crowe, J. (2002), An experimental study of the step-pool bed form, PhD thesis, Johns Hopkins Univ., Baltimore, Md.

Díaz, J., M. Ruíz, L. Crescentini, A. Amoruso, and J. Gallart (2014), Seismic monitoring of an alpine mountain river, *J. Geophys. Res. Solid Earth*, *119*, 3276–3289, doi:10.1002/2014JB010955.

Dietrich, W. E., J. W. Kirchner, H. Ikeda, and F. Iseya (1989), Sediment supply and the development of the coarse surface layer in gravel-bedded rivers, *Nature*, *340*(6230), 215–217.

Dunne, T., and L. B. Leopold (1978), *Water in Environmental Planning*, W. H. Freeman, New York.

Emmett, W. W., L. B. Leopold, and R. M. Myrick (1983), Some characteristics of fluvial processes in rivers, *U.S. Geol. Surv. Circ.*, *953*, 38.

Frings, R. M., and M. G. Kleinhans (2008), Complex variations in sediment transport at three large river bifurcations during discharge waves in the river Rhine, *Sedimentology*, *55*(5), 1145–1171, doi:10.1111/j.1365-3091.2007.00940.x.

Gee, D. M. (1975), Bed form response to nonsteady flows, *J. Hydraul. Div.*, *101*(3), 437–449.

Gimbert, F., V. C. Tsai, and M. P. Lamb (2014), A physical model for seismic noise generation by turbulent flow in rivers, *J. Geophys. Res. Earth Surf.*, *119*, 2209–2238, doi:10.1002/2014JF003201.

Gimbert, F., V. C. Tsai, J. M. Amundson, T. C. Bartholomaus, and J. I. Walter (2016), Sub-seasonal changes observed in subglacial channel pressure, size, and sediment transport, *Geophys. Res. Lett.*, *43*, 3786–3794, doi:10.1002/2016GL068337.

Golly, A., J. M. Turowski, A. Badoux, and N. Hovius (2017), Controls and feedbacks in the coupling of mountain channels and hillslopes, *Geology*, *45*(4), 307–310, doi:10.1130/G38831.1.

Govi, M., F. Maraga, and F. Moia (1993), Seismic detectors for continuous bed load monitoring in a gravel stream, *Hydrol. Sci. J.*, *38*(2), 123–132, doi:10.1080/02626669309492650.

Hegg, C. H., and D. Rickenmann (1999), Comparison of bedload transport in a steep mountain torrent with a bedload transport formula, in *Hydraulic Engineering for Sustainable Water Resources Management at the Turn of the Millennium, Proceedings 28th IAHR Congress*, p. 7, Technical Univ., Graz, Austria.

Hsu, L., N. J. Finnegan, and E. E. Brodsky (2011), A seismic signature of river bedload transport during storm events, *Geophys. Res. Lett.*, *38*, L13407, doi:10.1029/2011GL047759.

Humphries, R., J. G. Venditti, L. S. Sklar, and J. K. Wooster (2012), Experimental evidence for the effect of hydrographs on sediment pulse dynamics in gravel-bedded rivers, *Water Resour. Res.*, *48*, W01533, doi:10.1029/2011WR010419.

Julien, P., G. Klaassen, W. Ten Brinke, and A. Wilbers (2002), Case study: Bed resistance of Rhine river during 1998 flood, *J. Hydraul. Eng.*, *128*(12), 1042–1050, doi:10.1061/(ASCE)0733-9429(2002)128:12(1042).

Julien, P. Y., and B. Bounvilay (2013), Velocity of rolling bed load particles, *J. Hydraul. Eng.*, *139*(2), 177–186, doi:10.1061/(ASCE)HY.1943-7900.0000657.

Kean, J. W., J. A. Coe, V. Coviello, J. B. Smith, S. W. McCoy, and M. Arattano (2015), Estimating rates of debris flow entrainment from ground vibrations, *Geophys. Res. Lett.*, *42*, 6365–6372, doi:10.1002/2015GL064811.

Kleinhans, M., A. Wilbers, and W. Ten Brinke (2007), Opposite hysteresis of sand and gravel transport upstream and downstream of a bifurcation during a flood in the river Rhine, *Neth. J. Geosci.*, *86*(3), 273–285.

Klingeman, P., and W. Emmett (1982), Gravel bedload transport processes, in *Gravel-bed Rivers: Fluvial Processes, Engineering and Management*, edited by R. D. Hey, J. C. Bathurst, and C. R. Thornes, pp. 141–169, John Wiley, New York.

Kuhnle, R. A. (1992), Bed load transport during rising and falling stages on two small streams, *Earth Surf. Process. Landf.*, *17*(2), 191–197, doi:10.1002/esp.3290170206.

Lamb, M. P., W. E. Dietrich, and J. G. Venditti (2008), Is the critical shields stress for incipient sediment motion dependent on channel-bed slope?, *J. Geophys. Res.*, *113*, F02008, doi:10.1029/2007JF000831.

Mao, L. (2012), The effect of hydrographs on bed load transport and bed sediment spatial arrangement, *J. Geophys. Res.*, *117*, F03024, doi:10.1029/2012JF002428.

Mao, L., A. Dell'Agnese, C. Huincache, D. Penna, M. Engel, G. Niedrist, and F. Comiti (2014), Bedload hysteresis in a glacier-fed mountain river, *Earth Surf. Process. Landf.*, *39*(7), 964–976, doi:10.1002/esp.3563.

Martin, R. L., and D. J. Jerolmack (2013), Origin of hysteresis in bed form response to unsteady flows, *Water Resour. Res.*, *49*, 1314–1333, doi:10.1002/wrcr.20093.
Milhous, R., and P. Klingeman (1992), Bedload transport in mountain streams, in *Specialty Conference, American Society of Civil Engineers, Hydraulics Division*, Univ. of Iowa, Iowa City, Iowa.
Montgomery, D. R., and J. M. Buffington (1997), Channel-reach morphology in mountain drainage basins, *GSA Bull.*, *109*(5), 596–611, doi:10.1130/0016-7606(1997)109<0596:CRMIMD>2.3.CO;2.
Moog, D. B., and P. J. Whiting (1998), Annual hysteresis in bed load rating curves, *Water Resour. Res.*, *34*(9), 2393–2399, doi:10.1029/98WR01658.
Nanson, G. C. (1974), Bedload and suspended-load transport in a small, steep, mountain stream, *Am. J. Sci.*, *274*(5), 471–486, doi:10.2475/ajs.274.5.471.
Nitsche, M., D. Rickenmann, J. W. Kirchner, J. M. Turowski, and A. Badoux (2012), Macroroughness and variations in reach-averaged flow resistance in steep mountain streams, *Water Resour. Res.*, *48*, W12518, doi:10.1029/2012WR012091.
Paarlberg, A. J., C. M. Dohmen-Janssen, S. J. Hulscher, P. Termes, and R. Schielen (2010), Modelling the effect of time-dependent river dune evolution on bed roughness and stage, *Earth Surf. Process. Landf.*, *35*(15), 1854–1866, doi:10.1002/esp.2074.
Parker, G. (1990), Surface-based bedload transport relation for gravel rivers, *J. Hydraul. Res.*, *28*(4), 417–436, doi:10.1080/00221689009499058.
Reid, I., L. E. Frostick, and J. T. Layman (1985), The incidence and nature of bedload transport during flood flows in coarse-grained alluvial channels, *Earth Surf. Proc. Landforms*, *10*, 33–44, doi:10.1002/esp.3290100107.
Rickenmann, D. (2016), *Methods for the Quantitative Assessment of Channel Processes in Torrents (Steep Streams)*, CRC Press, Boca Raton, Fla.
Rickenmann D., and B. Fritschi (2010), Bedload transport measurements using piezoelectric impact sensors and geophones, in *Bedload-Surrogate Monitoring Technologies*, *U.S. Geol. Surv. Sci. Invest. Rep. 2010–5091*, edited by J. R. Gray, J. B. Laronne, and J. D. G. Marr, pp. 407–423, U.S. Geol. Surv., Reston, Va.
Rickenmann, D., and B. W. McArdell (2007), Continuous measurement of sediment transport in the Erlenbach stream using piezoelectric bedload impact sensors, *Earth Surf. Process. Landf.*, *32*(9), 1362–1378, doi:10.1002/esp.1478.
Rickenmann, D., and B. W. McArdell (2008), Calibration of piezoelectric bedload impact sensors in the Pitzbach mountain stream, *Geodin. Acta*, *21*(1–2), 35–52, doi:10.3166/ga.21.35-52.
Rickenmann, D., J. M. Turowski, B. Fritschi, A. Klaiber, and A. Ludwig (2012), Bedload transport measurements at the Erlenbach stream with geophones and automated basket samplers, *Earth Surf. Process. Landf.*, *37*(9), 1000–1011, doi:10.1002/esp.3225.
Rickenmann, D., J. M. Turowski, B. Fritschi, C. Wyss, J. Laronne, R. Barzilai, I. Reid, A. Kreisler, J. Aigner, H. Seitz, and H. Habersack (2014), Bedload transport measurements with impact plate geophones: Comparison of sensor calibration in different gravel-bed streams, *Earth Surf. Process. Landf.*, *39*(7), 928–942, doi:10.1002/esp.3499.
Roth, D., N. Finnegan, E. Brodsky, K. Cook, C. Stark, and H. Wang (2014), Migration of a coarse fluvial sediment pulse detected by hysteresis in bedload generated seismic waves, *Earth Planet. Sci. Lett.*, *404*, 144–153, doi:10.1016/j.epsl.2014.07.019.
Roth, D. L., E. E. Brodsky, N. J. Finnegan, D. Rickenmann, J. M. Turowski, and A. Badoux (2016), Bed load sediment transport inferred from seismic signals near a river, *J. Geophys. Res. Earth Surf.*, *121*, 725–747, doi:10.1002/2015JF003782.
Schmandt, B., R. C. Aster, D. Scherler, V. C. Tsai, and K. Karlstrom (2013), Multiple fluvial processes detected by riverside seismic and infrasound monitoring of a controlled flood in the Grand Canyon, *Geophys. Res. Lett.*, *40*, 4858–4863, doi:10.1002/grl.50953.
Schmandt, B., D. Gaeuman, R. Stewart, S. M. Hansen, V. C. Tsai, and J. Smith (2017), Seismic array constraints on reach-scale bedload transport, *Geology*, *45*(4), 299–302, doi:10.1130/G38639.1.
Schuerch, P., A. L. Densmore, B. W. McArdell, and P. Molnar (2006), The influence of landsliding on sediment supply and channel change in a steep mountain catchment, *Geomorphology*, *78*(3), 222–235, doi:10.1016/j.geomorph.2006.01.025.
Ten Brinke, W. B. M., A. W. E. Wilbers, and C. Wesseling (1999), Dune growth, decay and migration rates during a large-magnitude flood at a sand and mixed sand-gravel bed in the Dutch Rhine river system, in *Fluvial Sedimentology VI*, edited by N. D. Smith and J. Rogers, *Spec. Publ. Int. Assoc. Sedimentol.*, 28, 15–32, doi:10.1002/9781444304213.ch2.
Topping, D. J., D. M. Rubin, and L. E. Vierra (2000), Colorado River sediment transport: 1. Natural sediment supply limitation and the influence of Glen Canyon Dam, *Water Resour. Res.*, *36*(2), 515–542, doi:10.1029/1999WR900285.
Tsai, V. C., B. Minchew, M. P. Lamb, and J. P. Ampuero (2012), A physical model for seismic noise generation from sediment transport in rivers, *Geophys. Res. Lett.*, *39*, L02404, doi:10.1029/2011GL050255.
Turowski, J. M., E. M. Yager, A. Badoux, D. Rickenmann, and P. Molnar (2009), The impact of exceptional events on erosion, bedload transport and channel stability in a steppool channel, *Earth Surf. Process. Landf.*, *34*(12), 1661–1673, doi:10.1002/esp.1855.
Turowski, J. M., A. Badoux, and D. Rickenmann (2011), Start and end of bedload transport in gravel-bed streams, *Geophys. Res. Lett.*, *38*, L04401, doi:10.1029/2010GL046558.
Turowski, J. M., A. Badoux, J. Leuzinger, and R. Hegglin (2013a), Large floods, alluvial overprint, and bedrock erosion, *Earth Surf. Process. Landf.*, *38*(9), 947–958, doi:10.1002/esp.3341.
Turowski, J. M., M. Böckli, D. Rickenmann, and A. R. Beer (2013b), Field measurements of the energy delivered to the channel bed by moving bed load and links to bedrock erosion, *J. Geophys. Res. Earth Surf.*, *118*, 2438–2450, doi:10.1002/2013JF002765.
Turowski, J. M., C. R. Wyss, and A. R. Beer (2015), Grain size effects on energy delivery to the streambed and links to bedrock erosion, *Geophys. Res. Lett.*, *42*, 1775–1780, doi:10.1002/2015GL063159.
Walling, D. (1977), Assessing the accuracy of suspended sediment rating curves for a small basin, *Water Resour. Res.*, *13*(3), 531–538, doi:10.1029/WR013i003p00531.
Welch, P. D. (1967), The use of fast Fourier transform for the estimation of power spectra: A method based on time averaging over short, modified periodograms, *IEEE Trans. Audio Electroacoust.*, *15*(2), 70–73, doi:10.1109/TAU.1967.1161901.
Whiting, P. J., J. F. Stamm, D. B. Moog, and R. L. Orndorff (1999), Sediment-transporting flows in headwater streams, *GSA Bull.*, *111*(3), 450–466, doi:10.1130/0016-7606(1999)111<0450:STFIHS>2.3.CO;2.
Wiberg, P. L., and J. D. Smith (1991), Velocity distribution and bed roughness in high-gradient streams, *Water Resour. Res.*, *27*(5), 825–838, doi:10.1029/90WR02770.
Wilcock, P. R., and B. W. McArdell (1997), Partial transport of a sand/gravel sediment, *Water Resour. Res.*, *33*(1), 235–245, doi:10.1029/96WR02672.
Wijbenga, J., and G. Klaassen (1983), Changes in bedform dimensions under unsteady flow conditions in a straight flume, *Spec. Publ. Int. Assoc. Sedimentol.*, *6*, 35–48.
Wilbers, A., and W. Ten Brinke (2003), The response of subaqueous dunes to floods in sand and gravel bed reaches of the Dutch Rhine, *Sedimentology*, *50*(6), 1013–1034, doi:10.1046/j.1365-3091.2003.00585.x.
Winkler, W., W. Wildi, J. Van Stuijvenberg, and C. Caron (1985), Wägital-flysch et autres flyschs jenniques en suisse centrale. stratigraphie, sédimentologie et comparaisons, *Eclogae Geol. Helv.*, *7*(8), 1–22.

Wohl, E. E., and D. A. Cenderelli (2000), Sediment deposition and transport patterns following a reservoir sediment release, *Water Resour. Res.*, *36*(1), 319–333, doi:10.1029/1999WR900272.

Wulf, H., B. Bookhagen, and D. Scherler (2012), Climatic and geologic controls on suspended sediment flux in the Sutlej river valley, western Himalaya, *Hydrol. Earth Syst. Sci.*, *16*(7), 2193–2217, doi:10.5194/hess-16-2193-2012.

Wyss, C. R., D. Rickenmann, B. Fritschi, J. M. Turowski, V. Weitbrecht, and R. M. Boes (2016), Measuring bedload transport rates by grain size fraction using the Swiss plate geophone at the Erlenbach, *J. Hydraul. Eng.*, *142*(5), 1–11, doi:10.1061/(ASCE)HY.1943-7900.0001090.

Yager, E., J. Kirchner, and W. Dietrich (2007), Calculating bed load transport in steep boulder bed channels, *Water Resour. Res.*, *43*, W07418, doi:10.1029/2006WR005432.

Yager, E. M., W. E. Dietrich, J. W. Kirchner, and B. W. McArdell (2012a), Prediction of sediment transport in step-pool channels, *Water Resour. Res.*, *48*, W01541, doi:10.1029/2011WR010829.

Yager, E. M., J. M. Turowski, D. Rickenmann, and B. W. McArdell (2012b), Sediment supply, grain protrusion, and bedload transport in mountain streams, *Geophys. Res. Lett.*, *39*, L10402, doi:10.1029/2012GL051654.